An extended $E \otimes e$ Jahn-Teller Hamiltonian for large-amplitude motion: Application to vibrational conical intersections in CH_3SH and CH_3OH

Mahesh B. Dawadi, Bishnu P. Thapaliya, and David S. Perry

Citation: The Journal of Chemical Physics **147**, 044306 (2017); doi: 10.1063/1.4994699
View online: https://doi.org/10.1063/1.4994699
View Table of Contents: http://aip.scitation.org/toc/jcp/147/4
Published by the American Institute of Physics

An extended $E \otimes e$ Jahn-Teller Hamiltonian for large-amplitude motion: Application to vibrational conical intersections in CH_3SH and CH_3OH

Mahesh B. Dawadi, Bishnu P. Thapaliya,[a] and David S. Perry[b]
Department of Chemistry, The University of Akron, Akron, Ohio 44325-3601, USA

(Received 19 May 2017; accepted 6 July 2017; published online 26 July 2017)

An extended $E \otimes e$ Jahn-Teller Hamiltonian is presented for the case where the (slow) nuclear motion extends far from the symmetry point and may be described approximately as motion on a sphere. Rather than the traditional power series expansion in the displacement from the C_{3v} symmetry point, an expansion in the spherical harmonics is employed. Application is made to the vibrational Jahn-Teller effect in CH_3XH, with X = S, O, where the equilibrium CXH angles are 83° and 72°, respectively. In addition to the symmetry-required conical intersection (CI) at the C_{3v} symmetry point, *ab initio* calculations reveal sets of six symmetry-allowed vibrational CIs in each molecule. The CIs for each molecule are arranged differently in the large-amplitude space, and that difference is reflected in the infrared spectra. The CIs in CH_3SH are found in both eclipsed and staggered geometries, whereas those for CH_3OH are found only in the eclipsed geometry near the torsional saddle point. This difference between the two molecules is reflected in the respective high-resolution spectra in the CH stretch fundamental region. *Published by AIP Publishing.* [http://dx.doi.org/10.1063/1.4994699]

I. INTRODUCTION

The Jahn-Teller effect (JTE) was first formulated in the context of the spontaneous symmetry breaking of orbitally degenerate electronic states. The Jahn-Teller theorem states that "*A configuration of a polyatomic molecule for an electronic state having orbital degeneracy cannot be stable with respect to all displacements of the nuclei unless in the original configuration the nuclei all lie on a straight line.*"[1,2] In this context, the theoretical development was focused on relatively small displacements from a high-symmetry molecular configuration in which there were degenerate electronic states. Since then, it has been appreciated that the JTE has widespread applicability in both molecular spectroscopy and condensed-phase physics. In varied situations, "the JTE serves as an approved general model, which allows one to rationalize the results on molecular structure and properties obtained by other methods."[3] That is, the Jahn-Teller (JT) concept provides a general mathematical framework for treating a wide range of phenomena involving coupled adiabatic states.

In $E \otimes e$ systems, the relevant pair of states is degenerate (E) at the high-symmetry reference geometry (C_{3v} or D_{3h}). As the system is displaced from that high-symmetry geometry, the degenerate pair splits, which results in a symmetry-required conical intersection (CI) centered on the C_{3v} or D_{3h} reference geometry. In this work, we denote the displacement from the symmetrical geometry as ρ and the azimuthal (torsional) angle around the symmetry point as γ. We refer to JT coupling terms in $\exp(in\gamma)$ as nth-order JT coupling. Zwanziger and Grant[4] demonstrated that additional conical intersections between the JT-coupled adiabatic surfaces occur at large ρ when both the 1st- and 2nd-order JT couplings are active. Viel and Eisfeld[5,6] developed extended JT- and pseudo-JT-Hamiltonians that included polynomial coupling terms up to 6th order. Opalka and Domcke[7] have invoked invariant theory as a general means of deriving the symmetry-adapted polynomials needed for high-order JT Hamiltonians.

The vibrational JTE[8] extends the JT concept into the purely vibrational domain where certain vibrations with high frequencies are regarded as adiabatic functions of other low-frequency, large-amplitude coordinates. In the electronic domain, the potential energy surfaces (PESs) represent the adiabatic separation of electronic and nuclear motions under the Born-Oppenheimer approximation. In the vibrational domain, it is also possible to make a Born-Oppenheimer-like approximation separating fast and slow vibrational motions.[9–11] In this case, the motion of the high-frequency vibrations (e.g., OH, CH, CO, and SF stretches) can be adiabatically solved at each molecular geometry along the low-frequency coordinates such as torsion. The JT formalism is applicable when the resulting vibrationally adiabatic surfaces are degenerate at a symmetrical nuclear configuration in the large-amplitude vibrational coordinate space. Of course, the total adiabatic energy at each point in the large-amplitude space is the sum of the vibrationally adiabatic energy plus the energy of that nuclear configuration on the electronic PES.

In some cases of the vibrational JTE,[12] the electronic potential energy surface has a minimum-energy geometry that is far from $\rho = 0$. For example, in methanol, the minimum electronic energy occurs at a COH angle that is bent 72° from linear. In this case of the vibrational JTE, we take the two asymmetric CH stretch frequencies as adiabatic functions of the COH bend angle ρ and the torsional angle γ. When the COH angle is linear ($\rho = 0°$), the molecular geometry has C_{3v} symmetry and the two asymmetric CH stretches are degenerate. Although this symmetric geometry is rather

[a] Present address: Department of Chemistry, University of Tennessee, Knoxville, TN 37996, USA.
[b] Author to whom correspondence should be addressed: dperry@uakron.edu

high in energy (about 11 000 cm^{-1} above the minimum), it does serve as the reference point for the JT Hamiltonian. There are, however, additional molecular configurations distant from the symmetric geometry where the two asymmetric CH stretches become degenerate. These additional degeneracies are vibrational conical intersections that occur at much lower energies and are easily accessible to the low-energy dynamics.[12,13]

In our previous work,[12] the *ab initio* vibrationally adiabatic surfaces for methanol were fit to a JT Hamiltonian with JT coupling up to 4th order ($\cos 4\gamma$ coupling terms) and polynomial expansions in ρ with terms up to ρ^{16}. Although a precise fit to both the electronic and vibrational energies in methanol was obtained, some shortcomings of this form of the Hamiltonian were evident. First, the convergence properties of the long polynomial series in ρ were poor with substantial alternating positive and negative terms. Second, the polar coordinates (ρ,γ) were derived from the planar expansion in Cartesian coordinates, $x = \rho\cos\gamma$ and $y = \rho\sin\gamma$.[6] However, for a large range of ρ extending to 100°, such a planar representation neglects the curvilinear nature of the large-amplitude motion. At each (ρ, γ) combination, one finds that the optimized OH distance is roughly constant, so a better zeroth-order description of the large-amplitude space is the motion of H on a sphere centered at the O atom.

In this paper, we present a new formulation of the $E \otimes e$ Jahn-Teller Hamiltonian employing expansions of the diagonal potential and of the coupling terms in the spherical harmonics. This treatment facilitates application of the Jahn-Teller concept to systems where the relevant nuclear motions extend far from the relevant symmetry point. Application will be made to CH_3SH and CH_3OH where the domain of motion for the chalcogenic hydrogen is more than 2π steradians.

Starting with the first theoretical prediction by von Neumann and Wigner[14] in 1929, conical intersections (CIs) have been the subject of an enormous interest because of the key mechanistic role of CIs in photochemical and photophysical processes.[2,15,16] In electronic spectroscopy, CIs are true degeneracies of electronic PESs and are responsible for ultrafast electronic relaxation.[17–19] In the context of the vibrationally adiabatic approximation, vibrational CIs have been reported[12,13,20–23] and identified as a cause of ultrafast vibrational relaxation.[20–22]

In methanol,[12,13] there are seven related vibrational CIs between the vibrationally adiabatic surfaces that represent the energies of the first excited asymmetric CH stretch vibrations. One is at the symmetrical C_{3v} geometry where these two vibrations form a degenerate E-symmetry pair. The others are in the eclipsed configurations ($\gamma = 0°$, 120°, and 240°) near the top of the torsional barrier at $\rho = 62°$ and 92°. An obvious consequence of these vibrational CIs is the prediction of ultrafast energy transfer between the adiabatic surfaces and the expectation that the surface-hopping might be localized near the CIs.[12,13,17,20–22] The CIs provide a connection between the upper and lower surfaces where the system can transition smoothly from one surface to the other without any momentum gap in the low-frequency (ρ, γ) space. Hamm and Stock introduced the concept of vibrational CIs to demonstrate the ultrafast vibrational relaxation in different molecular systems and reported the time-dependent wavefunction propagation rate of ~100 fs for intra-molecularly H-bonded malonaldehyde and ~60 fs for the formate-water complex.[20,21]

In this paper, we add methyl mercaptan (CH_3SH), the thiol analog of methanol, as an additional example of a system with multiple vibrational CIs; however, the pattern of those CIs in the large-amplitude space is rather different from methanol.

II. A JAHN-TELLER HAMILTONIAN FOR LARGE-AMPLITUDE MOTION

The premise of the Jahn-Teller effect is a partition of the degrees of freedom in a molecular system into fast (f) and slow (s) degrees of freedom. The fast degrees of freedom could correspond to electronic motion or—as in the examples we present here—to high-frequency vibrations. We are interested in situations where the slow coordinates $\bar{Q} = (\rho, \gamma)$ represent large-amplitude motion that may be described approximately as motion on the surface of a sphere. Examples include the torsional and bending motions of the chalcogenic proton in CH_3XH with X = O, S. In these cases, the large-amplitude coordinates are the CXH bend (ρ) and the symmetrized[24] torsional angle (γ).

The Hamiltonian can be written as the sum of two parts,

$$H = H_f + T_s. \tag{1}$$

In this paper, the slow coordinates are taken to be the usual spherical polar angles, $\bar{Q} \equiv (\rho, \gamma)$. The kinetic energy operator for these slow degrees of freedom is then $T_s = L^2/2\mu r^2$, where L^2 is the usual orbital angular momentum operator, μ is the reduced mass, and r is the radius of the sphere. The Hamiltonian H_f for the fast degrees of freedom includes all contributions to the potential energy plus the kinetic energy operator for the fast degrees of freedom.

The eigenfunctions ψ_f of H_f are determined by

$$H_f\psi_f = E_f\left(\bar{Q}\right)\psi_f, \tag{2}$$

where both $H_f = H_f\left(\bar{q};\bar{Q}\right)$ and $\psi_f = \psi_f\left(\bar{q};\bar{Q}\right)$ are explicit functions of the fast coordinates, $\bar{q}$, and parametric functions of the slow coordinates, $\bar{Q}$. Equation (2) is solved at each combination of the slow coordinates and the resulting fast eigenvalues $E_f\left(\bar{Q}\right)$ are also the functions of ρ and γ.

In the $E \otimes e$ Jahn-Teller problem, we focus on a pair of fast states (E) that are degenerate at the C_{3v} (or D_{3h}) reference geometry and consider their dependence on the pair of slow coordinates (e). Here, for the fast degrees of freedom, the crude adiabatic basis[4] will be used, and the basis set will be restricted to the two E-type functions, $\phi_{f,x}$ and $\phi_{f,y}$, in the Cartesian (real) representation. This Cartesian basis is related to the commonly used complex representation by a unitary transformation.[6] The Hamiltonian matrix becomes

$$H_f = \begin{bmatrix} H_{f,xx} & H_{f,xy} \\ H_{f,yx} & H_{f,yy} \end{bmatrix}, \tag{3}$$

where

$$H_{f,ij}\left(\bar{Q}\right) = \left\langle \phi_{f,i}|H_f|\phi_{f,j}\right\rangle_{\bar{q}}, \text{ with } i = x, y \text{ and } j = x, y. \tag{4}$$

Here, the integration over the fast coordinates is indicated as a subscript $\bar{q}$, and the dependence of the result on the slow coordinates $\bar{Q}$ is indicated explicitly.

The overall Schrödinger equation

$$H\psi = E\psi \tag{5}$$

can then be solved in a product basis,

$$\Phi_{ki} \equiv \phi_{s,k}\phi_{f,i}. \tag{6}$$

The Hamiltonian matrix elements in this product basis are then

$$\left\langle \Phi_{ki}|H|\Phi_{lj}\right\rangle_{\bar{Q},\bar{q}} = \left\langle \phi_{s,k}|H_{f,ij}|\phi_{s,l}\right\rangle_{\bar{Q}} + \left\langle \phi_{s,k}|T_{s,ij}|\phi_{s,l}\right\rangle_{\bar{Q}}. \tag{7}$$

Here, the slow basis functions ϕ_s form a complete set in the slow coordinate space, and the indices k and l label the members of that complete set. The indices i and j label the fast basis functions ϕ_f as above. The subscripts $\bar{Q}$ and $\bar{q}$ indicate integrations over the slow and fast coordinates, respectively.

For nonzero contributions to Eq. (7), the integrands must be totally symmetric; that is, in terms of the symmetry species in C_{3v}, we require

$$a_1 \sqsubset \Gamma\left(\phi_{s,k}\right) \otimes \Gamma\left(H_{f,ij}\right) \otimes \Gamma\left(\phi_{s,l}\right). \tag{8}$$

Since $\Gamma\left(\phi_{s,k}\right) = \Gamma\left(\phi_{s,l}\right) = e$, we must have $\Gamma\left(H_{f,ij}\right) = a_1 \oplus e$. We represent the terms of these two symmetries as

$$H_f = H_f^{a1} + H_f^e = \begin{bmatrix} H_{f,xx}^{a1} & H_{f,xy}^{a1} \\ H_{f,yx}^{a1} & H_{f,yy}^{a1} \end{bmatrix} + \begin{bmatrix} H_{f,xx}^{e} & H_{f,xy}^{e} \\ H_{f,yx}^{e} & H_{f,yy}^{e} \end{bmatrix}. \tag{9}$$

In this work, we use e-type basis functions that transform as the Cartesian x- and y-components of the degenerate representation. To assure consistency in the handling of the e-symmetry terms in the Hamiltonian [Eq. (9)], it is useful to consider the C_s subgroup of C_{3v} that has the x-z plane as its plane of symmetry and in which the x- and y-components of the e species transform, respectively, as a' and a''. The requirement of totally symmetric (a') integrands then gives the following species in C_s for the matrix elements in Eq. (9):

$$\begin{aligned} a' &: H_{f,xx}^{a1}, H_{f,yy}^{a1}, H_{f,xx}^{e}, H_{f,yy}^{e}, \\ a'' &: H_{f,xy}^{e}, H_{f,yx}^{e}, \end{aligned} \tag{10}$$

and $$H_{f,xy}^{a1} = H_{f,yx}^{a1} = 0.$$

The requirement that the eigenvalues of H_f be invariant to any unitary transformation gives $H_{f,xx}^{a1} = H_{f,yy}^{a1} \equiv H_f^{a1}$, $H_{f,xx}^{e} = -H_{f,yy}^{e}$, and $H_{f,xy}^{e} = H_{f,yx}^{e}$. This yields H_f in the same form which is given in Eq. (9) of Ref. 6,

$$H_f = \begin{bmatrix} H_f^{a1} & 0 \\ 0 & H_f^{a1} \end{bmatrix} + \begin{bmatrix} H_{f,xx}^{e} & H_{f,xy}^{e} \\ H_{f,xy}^{e} & -H_{f,xx}^{e} \end{bmatrix}. \tag{11}$$

Each of these matrix elements is a function of the slow coordinates $\bar{Q} = (\rho, \gamma)$ and we expand them in the spherical harmonics,

$$H_{f,ij}^{\Gamma}(\rho,\gamma) = \sum\nolimits_{l,m} c_{lm}^{\Gamma} Y_{lm}(\rho,\gamma). \tag{12}$$

Here, Y_{lm} are the real combinations of the complex spherical harmonics, where the functions containing $\cos(m\gamma)$ are denoted with the index $m > 0$ and those containing $\sin(|m|\gamma)$ are denoted with $m < 0$. The former transform as a' in C_s and the latter as a''. The symmetries of the spherical harmonics in C_{3v} are given by Altman and Bradley.[25] For a_1, only the $m = 0$, 3, 6, ... coefficients in Eq. (12) are non-zero. For e, we label the coefficients as c_{lm}^{exx} and c_{lm}^{exy} as needed to distinguish the a' and a'' components, respectively. We have then $c_{lm}^{exx} \equiv c_{lm}^{e} \neq 0$ only for $m = 1, 2, 4, 5, 7, \ldots$, and $c_{l,-m}^{exy} = \pm c_{lm}^{e}$ with the upper sign applicable to $m = 1, 4, 7, \ldots$, and the lower sign otherwise. The expansion in Eq. (12) includes all values of l for $l \geq |m|$.

Viel and Eisfeld[6] expanded the Hamiltonian in Eq. (11) in Cartesian coordinates, $\bar{Q} = (x, y)$ and derived the Jahn-Teller coupling terms up to 6th order. Thapaliya *et al.*[12] expressed this expansion in polar coordinates $\bar{Q} = (\rho, \gamma)$ resulting in a Fourier expansion in γ and a power series in ρ. They extended the expansion, including polynomial terms in ρ up to ρ^{16} in certain of the fits to *ab initio* data. In the limit in which that expansion is carried to all orders, it is exactly equivalent to the present expansion given by Eq. (12). The only difference arises when the respective infinite series are truncated as is always necessary in a practical situation. The spherical harmonics in Eq. (12) contain sines and cosines of ρ, which in turn might be expanded as infinite power series in ρ. Any truncation of Eq. (12) then keeps some contribution from very high-order polynomial terms that would be truncated in a finite power series expansion. Whereas any finite power series expansion diverges for large ρ, the spherical harmonics are finite everywhere. As we will show below, the result is better behaved fits yielding a reduced mean square error with the same number of expansion terms.

For the present application to the vibrational Jahn-Teller effect, it is convenient to write the diagonal (a_1) terms as the sum of electronic (U) and vibrational (V) parts,

$$H_f^{a1} = U + V. \tag{13}$$

As before,[12] we group both the diagonal and the off-diagonal terms as Fourier series in γ. We refer to the collectivity of the coupling terms in $\cos m\gamma$ and $\sin m\gamma$ as mth-order Jahn-Teller coupling. The relevant Fourier expansions are then

$$U = U^{0\gamma} + U^{3\gamma}\cos 3\gamma + U^{6\gamma}\cos 6\gamma + \cdots, \tag{14}$$

$$V = V^{0\gamma} + V^{3\gamma}\cos 3\gamma + V^{6\gamma}\cos 6\gamma + \cdots, \tag{15}$$

$$H_{f,xx}^{e} = W^{1\gamma}\cos\gamma + W^{2\gamma}\cos 2\gamma + W^{4\gamma}\cos 4\gamma + \mathrm{W}^{5\gamma}\cos 5\gamma + \cdots, \tag{16}$$

$$H_{f,xy}^{e} = W^{1\gamma}\sin\gamma - W^{2\gamma}\sin 2\gamma + W^{4\gamma}\sin 4\gamma - W^{5\gamma}\sin 5\gamma + \cdots, \tag{17}$$

where the Fourier coefficients are

$$U^{m\gamma}(\rho) = \sum_{l=m,m+1,\ldots} b_{lm}^{a1}\frac{Y_{lm}(\rho,\gamma)}{\cos m\gamma}, \tag{18}$$

$$V^{m\gamma}(\rho) = \sum_{l=m,m+1,\ldots} c_{lm}^{a1}\frac{Y_{lm}(\rho,\gamma)}{\cos m\gamma}, \tag{19}$$

$$W^{m\gamma}(\rho) = \sum_{l=m,m+1,\ldots} c_{lm}^{e}\frac{Y_{lm}(\rho,\gamma)}{\cos m\gamma}. \tag{20}$$

In Eqs. (18)–(20), the only non-zero terms are those allowed by symmetry, that is, $m = 0$, 3, 6, ... for $U^{m\gamma}$ and $V^{m\gamma}$ and

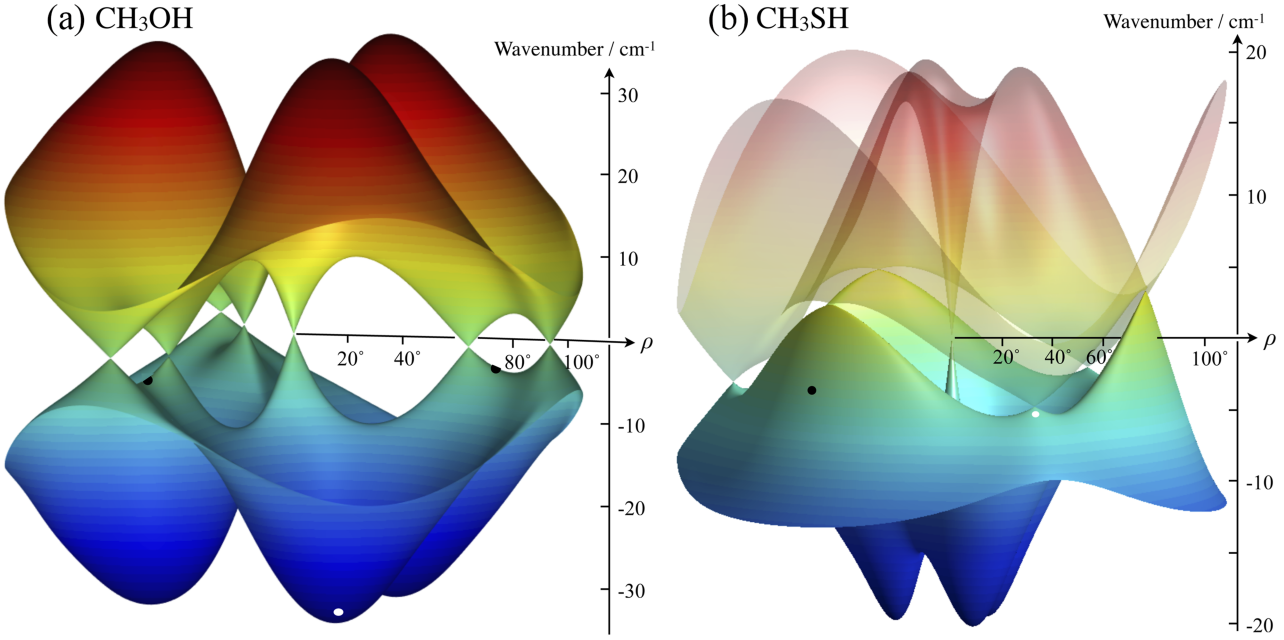

FIG. 1. For CH_3OH (a) and CH_3SH (b), the relative asymmetric CH stretch frequencies (vertical coordinate) are represented in the (horizontal) 2-dimensional coordinate space of CSH bend angle ρ (radial coordinate) and the torsional angle γ (polar angle). These vibrationally adiabatic surfaces are fits of the *ab initio* data [CCSD(T)/aug-cc-pVTZ] to the extended Jahn-Teller Hamiltonian. For each molecule, the adiabatic surfaces meet in several conical intersections, one at $\rho = 0$ and six others for $\rho > 0$. The $V^{0\gamma}$ Fourier terms, as well as the entire electronic potential energy (U), have been suppressed in the figure for better viewability. The white dots indicate the location of global minima of the electronic potential; the black dots indicate the location of torsional saddle points.

m = 1, 2, 4, 5, ... for $W^{m\gamma}$. The coefficient b^{a1}_{lm} has been introduced in Eq. (18) to distinguish the coefficients for the electronic energy from those for the vibrational energy.

The eigenvalues of Eq. (2) are readily obtained. For example, including terms up to $m = 6$ for $U^{m\gamma}$ and $V^{m\gamma}$ and up to $m = 4$ for $W^{m\gamma}$, one gets

$$E_{f\pm}(\rho,\gamma) = \left(V^{0\gamma} + U^{0\gamma}\right) + \left(V^{3\gamma} + U^{3\gamma}\right)\cos 3\gamma + \left(V^{6\gamma} + U^{6\gamma}\right) \times \cos 6\gamma \pm \{(W^{1\gamma})^2 + (W^{2\gamma})^2 + (W^{4\gamma})^2 + 2W^{1\gamma} \times \left(W^{2\gamma} + W^{4\gamma}\right)\cos 3\gamma + 2W^{2\gamma}W^{4\gamma}\cos 6\gamma\}^{1/2} \quad (21)$$

Each of the Fourier coefficients $U^{m\gamma}$, $V^{m\gamma}$, and $W^{m\gamma}$ appearing in Eq. (21) is the one-dimensional function of ρ as defined in Eqs. (18)–(20). These fast eigenvalues, when plotted in the large-amplitude space, constitute adiabatic surfaces. Examples of adiabatic surfaces that obey Eq. (21) are shown in Fig. 1. The specifics of how these surfaces were obtained are detailed in Secs. III–V.

Conical intersections between the adiabatic surfaces (Fig. 1) occur wherever the Jahn-Teller coupling terms, $H^e_{f,xx}$ [Eq. (16)] and $H^e_{f,xy}$ [Eq. (17)], are both zero. In the absence of the Jahn-Teller effect, the crude adiabatic basis states employed here are degenerate everywhere in the (ρ, γ) large-amplitude space. The term $H^e_{f,xx}$ produces a diagonal splitting of the basis states and $H^e_{f,xy}$ is the off-diagonal coupling. In general, CIs can be grouped into three categories. The first category is symmetry-required CIs, exemplified by the CI at the C_{3v} geometry ($\rho = 0$) where both terms are necessarily zero by symmetry [$Y^m_l(0,0) = 0$ for $m \neq 0$]. The second category is symmetry-allowed CIs, for which the off-diagonal coupling $H^e_{f,xy}$ is zero by symmetry and the diagonal splitting $H^e_{f,xx}$ is zero accidentally. In the present case, the symmetry-allowed CIs occur in the planes of symmetry, that is, either in the staggered ($\gamma = 60°, 180°, 300°$) or eclipsed ($\gamma = 0°, 120°, 240°$) conformations. In the staggered conformation, CIs occur at values of ρ where

$$\sum_m (-1)^m W^{m\gamma}(\rho) = 0 \quad (22)$$

and in the eclipsed conformation where

$$\sum_m W^{m\gamma}(\rho) = 0. \quad (23)$$

Finally, the third category is fully accidental CIs that occur in non-symmetric conformations at coordinates (ρ, γ) where both criteria are met accidentally. This paper focuses on the six symmetry-allowed CIs in each of the subject molecules, but, as yet, we have not found any fully accidental CIs for a C_{3v} molecule.

III. COMPUTATIONAL METHODS

Ab initio molecular structure methods are used to obtain approximations to the adiabatic eigenvalues E_f [Eq. (2)] for the fast degrees of freedom. In the present computations on CH_3SH, the fast degrees of freedom are the two asymmetric CH stretch vibrations. The adiabatic energies of the CH stretch excited states are computed at constrained points $\bar{Q} = (\rho, \gamma)$ in the large-amplitude space. The set of adiabatic eigenvalues $E_{f\pm}(\rho, \gamma)$ is then fit to the Jahn-Teller Hamiltonian as parameterized in Eqs. (11) and (12) and exemplified by Eq. (21). The computational methods and approximations used

have been documented[12] and are summarized only briefly here.

The *ab initio* calculations are partially optimized calculations in which the values of $\bar{Q} = (\rho, \gamma)$ are constrained and all of the other 10 vibrational coordinates are optimized to yield a minimum of the electronic potential energy, $U(\rho, \gamma)$. The vibrational contributions to the eigenvalues $E_{f\pm}$, measured relative to the zero-point level, are approximated by the harmonic frequencies of the two fast normal modes as calculated by the G09 electronic structure package.[26] Two of the normal modes are well described as asymmetric CH stretches, and, as we have shown previously for methanol,[12] the admixture of the other internal coordinates in those normal modes does not have a significant impact on the present results. The results presented in this paper, both for the partial optimizations and for the frequency calculations, were obtained at the CCSD(T)/aug-cc-pVTZ level with "very tight" convergence unless specifically noted. We will show below that results obtained at two lower levels are close to those obtained at this level. For CH_3SH, the computed stationary points on the electronic potential energy surfaces are the global minima (ρ = 83.32°, γ = 60°, 180°, 300°), the torsional saddle points (ρ = 83.01°, γ = 0°, 120°, 240°), and the C_{3v} symmetry point ($\rho = 0$).

IV. VIBRATIONALLY ADIABATIC SURFACES

A. Vibrational conical intersections in CH_3SH

Computed frequencies for the asymmetric CH stretches are shown in Fig. 2(a) for the staggered (*s*) and eclipsed (*e*) conformations of CH_3SH. At $\rho = 0°$, in the C_{3v} geometry, the two asymmetric CH stretches are a degenerate *E*-type vibration. In the staggered conformation for small ρ, the A' frequency is higher, but then at ρ = 79.0°, it crosses the A'' frequency to become lower. In the eclipsed conformation, there is a crossing in the reverse direction at 70.65°. These crossings are places where the two asymmetric CH stretches become degenerate, and when viewed in the context of the 2-D large-amplitude coordinate space (ρ, γ), they are vibrational conical intersections (CIs). The crossing at $\rho = 0$ constitutes a symmetry-required CI. For $\rho > 0$, the crossings are symmetry-allowed CIs because the coupling between the A' and A'' vibrations is necessarily zero in the planes of symmetry that contain the staggered and eclipsed conformations.

Away from the C_s planes, the coupling becomes nonzero and the CH stretch vibrations split further apart. A full listing of the *ab initio* results on CH_3SH is given in Tables S1 and S2 of the supplementary material. These data include the data of Fig. 2 plus 26 *ab initio* points in non-C_s geometries. These non-C_s points are located near the crossings of two frequencies, along the torsional minimum energy path (MEP), and at γ = 30°. To assure the correct symmetry of the results, the symmetrized torsional angles were employed[12] for all non-C_s geometries. As was done previously,[12] the computed harmonic vibrational frequencies were used as approximations to the energies of the quantum mechanical vibrationally excited states relative to the zero-point vibrational level. In this context, these computed CH-stretch vibrational frequencies constitute points on the vibrationally adiabatic potential energy surface.

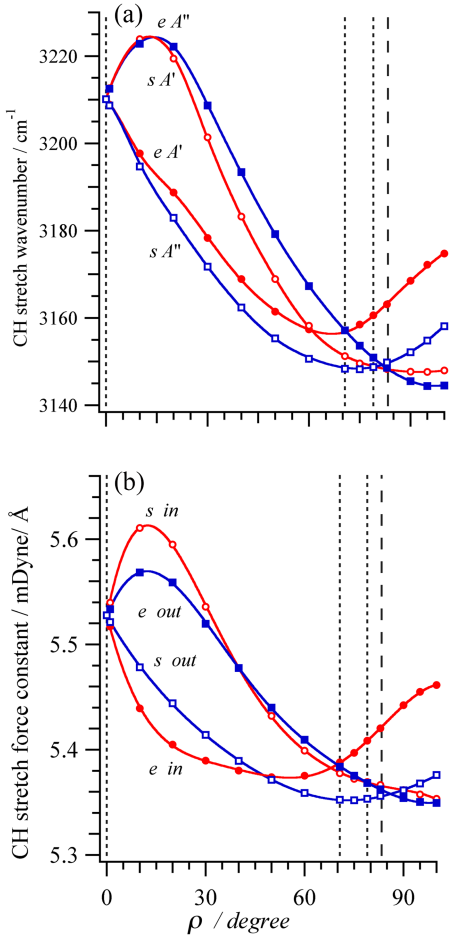

FIG. 2. (a) Markers indicate the vibrational frequencies for the two asymmetric CH stretch vibrations ν_1 (A′) and ν_9 (A″) of CH_3SH computed at the *ab initio* level CCSD(T)/aug-cc-pVTZ for conformations of C_s symmetry. The abscissa is the CSH bend angle ρ, measured relative to linearity ($\rho = 0$). The staggered (*s*) and eclipsed conformations (*e*) are indicated. In (a), the lines are the global fit to the extended Jahn-Teller Hamiltonian. (b) Markers indicate the harmonic force constants for individual CH bonds in the C_s plane of symmetry (*in*) and out-of-plane (*out*) cross at nearly the same ρ angles. In (b), the lines are simply smooth curves connecting the markers. The vertical lines, extending through both parts of the figure, indicate the ρ angles at which the A′ and A″ frequencies cross (short-dashed lines) and also the equilibrium geometry (long-dashed lines).

The locations of the seven CIs in CH_3SH provide a test of the computational level dependence of the results. The three molecular structure levels tested are (i) DFT/B3LYP/6-31+(2d,p), (ii) MP2(full)/6-311+(3df,2p), and (iii) CCSD(T)/aug-cc-pVTZ. The locations of the global minima and torsional saddle points varied within a range $\Delta\rho \leq 0.4°$ across the three levels. The locations of the CIs for the MP2 and CCSD(T) levels agree to within $\Delta\rho = 0.4°$. A larger difference was found between the B3LYP and CCSD(T) levels, with the staggered CIs found at 6° larger ρ in the B3LYP calculation. The qualitative pattern of the data, such as those shown in Fig. 2, was similar in all three calculations. The details of the computational level dependence are given in Table S3 of the supplementary material. We find that the phenomenon of the vibrational CIs and their qualitative pattern is evident even at the lowest level of calculation. An understanding of the phenomenon can be found in Fig. 2(b). One sees there that the variation of the single-bond CH stretch force constants is

similar to the variation of the relevant CH stretch normal mode frequencies. Thus, the vibrational CIs arise primarily from the variation of the single-bond CH-stretch force constants in the large-amplitude space.

B. Energy surfaces and fitting parameters

As a practical matter, fitting the *ab initio* adiabatic energies $E_{f\pm}(\rho,\gamma)$ to the Jahn-Teller Hamiltonian as given by Eqs. (11)–(21) faces some challenges. First, the surfaces represented by $E_{f\pm}(\rho,\gamma)$ are complicated containing several vibrational conical intersections where the two surfaces become degenerate. Second, many parameters, typically a few dozen, are required for a good fit. Finally, a fit to an eigenvalue expression such as Eq. (21) employs an iterative nonlinear least squares algorithm. In the present case, very good initial values of the parameters are required for the fit to converge correctly. Fortunately, an excellent set of initial values may be obtained by reducing the fit of the 2-dimensional (ρ,γ) data to Eq. (21), to a series of 1-dimensional fits to Eqs. (18)–(20). As was done before,[12] explicit values of each of the Fourier terms in Eq. (21) may be obtained as appropriate linear combinations of the *ab initio* electronic and vibrational energies obtained for a given value of ρ at $\gamma = 0°$, 30°, and 60°. That is, $U^{m\gamma}(\rho)$, $V^{m\gamma}(\rho)$, and $W^{m\gamma}(\rho)$ for discrete values of ρ (Fig. 3) are obtained directly from the *ab initio* data, and then each is fit as a 1-D function to Eqs. (18)–(20) to obtain initial values of the parameters, b^{a1}_{lm}, c^{a1}_{lm}, and c^{e}_{lm}. Then, with these initial values, the global nonlinear fit of Eq. (21) to the entire available dataset is executed to obtain precise fits and final parameters that are very close to these initial values.

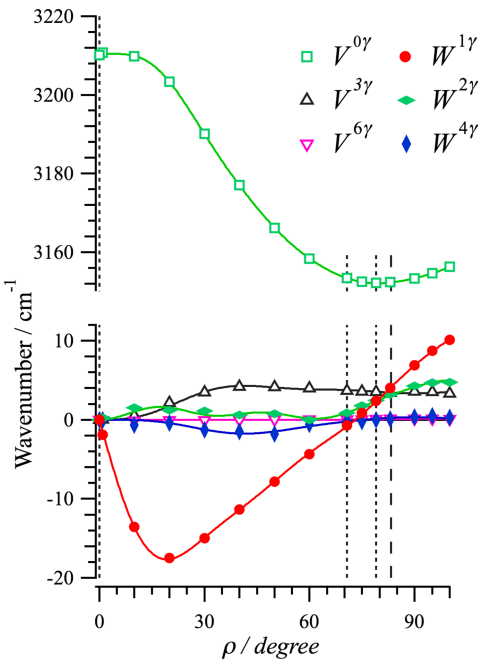

FIG. 3. Fourier terms of the Jahn-Teller model Hamiltonian [Eqs. (19) and (20)] for CH_3SH as the function of the CSH bending angle ρ. The markers are calculated directly from the CCSD(T)/aug-cc-pVTZ *ab initio* data at specific values of ρ. The curves represent the global fit to Eq. (21). The vertical short-dashed lines indicate the locations of the vibrational conical intersections (CIs), and the vertical long-dashed line indicates the value of ρ at the global minima of the electronic potential.

The *ab initio* data on CH_3SH are well fit by the extended Jahn-Teller Hamiltonian in the form of Eqs. (18)–(21). For convenience, the electronic potential energy surface [Eqs. (14) and (18)] was fit separately from the vibrational energies [the remaining contributions to Eq. (21)]. The global fit parameters are listed in Table I. The fit residuals are tabulated along with the *ab initio* data in Tables S1 and S2 of the supplementary material.

The fitted vibrationally adiabatic surfaces for CH_3SH as shown in Fig. 1(b) exhibit seven conical intersections. The symmetry-required CI occurs at the C_{3v} reference geometry ($\rho = 0°$). Three symmetry-allowed CIs occur at $\rho = 79.0°$ in the staggered conformations, and three more in the eclipsed conformations at $\rho = 70.65°$. The CIs at $\rho = 79°$ are very close to the global minimum electronic energy ($\rho = 83.3°$), within the range of zero-point C–S–H bending amplitude. These CIs occur at low energies and therefore will impact the molecular dynamics even in the ground state of the large-amplitude vibrations. The CIs in the eclipsed conformation at $\rho = 70.65°$ are close to the torsional saddle points ($\rho = 83.0°$), which means that these CIs are also accessible at relatively low energies and are within the range of C–S–H zero-point bending amplitude. By contrast, the CI at the C_{3v} symmetry point ($\rho = 0°$) occurs at a second-order saddle point on the electronic potential energy surface, about 24 000 cm^{-1} above the global minima and well out of the reach of the low-energy dynamics.

The adiabatic surfaces for CH_3OH can be compared to those for CH_3SH in Fig. 1. For consistency, the CH_3OH *ab initio* data at the same CCSD(T) level[12] were re-fit to the present extended Hamiltonian [Eqs. (11)–(21)]. Both molecules have 6 symmetry-allowed vibrational CIs, but their arrangement in the large-amplitude (ρ,γ) coordinate space is rather different. In CH_3OH, the CIs occur in both the staggered and eclipsed conformations, but in methanol, the CIs are found only in the eclipsed conformation at $\rho = 62°$ and 92°. In methanol, CIs at $\rho = 62°$ are near the torsional saddle points and are accessible at relatively low energies within the range of COH zero-point bending amplitude.

V. DISCUSSION

The present expansion of the Jahn-Teller Hamiltonian in terms of the spherical harmonics may be compared to our earlier work[12] in which the same Hamiltonian was expanded in a power series in the CXH angle ρ. The expansion in the torsional angle γ is the same for both. For CH_3OH, with the same number of terms (17 for the electronic part and 38 for the vibrational part), the spherical harmonic expansion gave an overall RMS error of 0.21 cm^{-1} as compared to 0.57 cm^{-1} reported earlier.[12] We were not able to satisfactorily fit the electronic part of the potential energy for CH_3SH with the polynomial expansion, which is what prompted us to develop the spherical harmonic approach. In CH_3SH, the electronic energy of the C_{3v} geometry is 24 000 cm^{-1} above the global minimum as compared to 11 000 cm^{-1} for CH_3OH. To fit the CH_3SH electronic potential to the same precision as for CH_3OH, many more terms were required, which resulted in spurious oscillations. In the present fits, the spherical harmonic expansion with the same number of terms does nearly as well

TABLE I. Jahn-Teller parameters for CH_3SH.

Fourier term[a]	Parameter[b]	Value[c]	Fourier term[a]	Parameter[b]	Value[c]
$U^{0\gamma}$	b^{a1}_{00}	33 009.50 (36)	$V^{0\gamma}$	c^{a1}_{00}	11 245.30 (0.5)
	b^{a1}_{10}	−15 062.20 (50)		c^{a1}_{10}	−24.20 (0.6)
	b^{a1}_{20}	30 758.00 (41)		c^{a1}_{20}	70.84 (0.3)
	b^{a1}_{30}	−2 049.77 (23)		c^{a1}_{40}	10.52 (0.11)
	b^{a1}_{40}	3 423.75 (7)		c^{a1}_{80}	−0.60 (0.10)
	b^{a1}_{60}	842.11 (1.0)		c^{a1}_{100}	−1.20 (0.09)
	b^{a1}_{80}	279.80 (0.3)		c^{a1}_{120}	−0.50 (0.09)
	b^{a1}_{100}	105.72 (0.19)		c^{a1}_{140}	−0.23 (0.09)
	b^{a1}_{120}	40.50 (0.16)	$V^{3\gamma}$	c^{a1}_{33}	7.89 (0.17)
	b^{a1}_{140}	16.32 (0.15)		c^{a1}_{43}	0.12 (0.20)
	b^{a1}_{160}	7.09 (0.13)		c^{a1}_{53}	3.79 (0.16)
	b^{a1}_{180}	2.05 (0.09)		c^{a1}_{73}	1.74 (0.10)
$U^{3\gamma}$	b^{a1}_{33}	598.82 (2)		c^{a1}_{93}	0.61 (0.09)
	b^{a1}_{43}	−195.96 (3)		c^{a1}_{113}	0.13 (0.03)
	b^{a1}_{53}	290.25 (2)	$V^{6\gamma}$	c^{a1}_{66}	0.07 (0.02)
	b^{a1}_{73}	30.21 (1.6)		c^{a1}_{76}	−0.02 (0.03)
	b^{a1}_{83}	13.64 (1.7)	$W^{1\gamma}$	c^{e}_{11}	9.24 (0.2)
	b^{a1}_{93}	17.68 (0.8)		c^{e}_{21}	−19.79 (0.3)
	b^{a1}_{113}	2.54 (0.07)		c^{e}_{31}	−2.88 (0.06)
	b^{a1}_{133}	3.67 (0.15)		c^{e}_{51}	−6.38 (0.09)
	b^{a1}_{153}	0.49 (0.04)		c^{e}_{71}	−2.92 (0.08)
	b^{a1}_{173}	0.65 (0.12)		c^{e}_{91}	−1.15 (0.07)
$U^{6\gamma}$	b^{a1}_{66}	−0.12 (0.03)		c^{e}_{111}	−0.22 (0.02)
	b^{a1}_{86}	−0.57 (0.03)	$W^{2\gamma}$	c^{e}_{22}	3.98 (0.11)
				c^{e}_{42}	−4.14 (0.2)
				c^{e}_{52}	2.58 (0.15)
Calculation method		CCSD(T)		c^{e}_{102}	0.69 (0.09)
Basis set		aug-cc-pVTZ		c^{e}_{122}	0.27 (0.08)
RMS (vibrational)[d]		0.20	$W^{4\gamma}$	c^{e}_{54}	−0.65 (0.14)
RMS (overall)[d]		0.26		c^{e}_{64}	−0.75 (0.15)
				c^{e}_{104}	0.24 (0.10)

[a]The Fourier terms $U^{m\gamma}$, $V^{m\gamma}$, and $W^{m\gamma}$ are defined in Eqs. (14)–(20).
[b]The parameters b^{Γ}_{lm} were fit to 54 *ab initio* points on the electronic potential, and c^{Γ}_{lm} were fit to corresponding 108 values of the asymmetric CH stretch vibrational frequencies. Parameters omitted from this table were set to zero because they did not improve the quality of the fit.
[c]Both the parameter values and their uncertainties in parentheses are given in cm^{-1} units.
[d]Root-mean-square errors of the fits. The RMS (overall) includes contributions from both the vibrational and electronic fits.

(overall RMS 0.26 cm^{-1}) for CH_3SH as it does for CH_3OH, and without any spurious oscillations. Also for values of ρ greater than represented in the *ab initio* data, a high-order polynomial expansion quickly diverges toward ± infinity, whereas the spherical harmonics remain finite everywhere.

An important difference between the two approaches stems from the origin of the power series Hamiltonian as an expansion in planar nuclear coordinates, (x, y),[6] which can be expressed in terms of the planar polar coordinates $\bar{Q} = (\rho, \gamma)$. In the present context where the distance of the XH proton from the X atom is roughly constant, large-amplitude motion is better described as motion on a sphere than motion in a plane, and we identify $\bar{Q} = (\rho, \gamma)$ as the spherical polar angles. The expansion in spherical harmonics takes advantage of this approximate description of the curvilinear nature of the large-amplitude motion. Of course when ρ remains small, the motion is nearly planar and the traditional low-order power series expansion is quite adequate.

The asymmetric CH stretches in both CH_3SH and CH_3OH and their variation in the large-amplitude space are well described by the Jahn-Teller Hamiltonian and both exhibit multiple vibrational conical intersections accessible at relatively low energy. However the pattern of the CIs [Figs. 1(a) and 1(b)] is quite different from all of the CIs confined to eclipsed geometries in CH_3OH. In CH_3OH, the 1st- and 2nd-order Jahn-Teller interactions ($W^{1\gamma}$ and $W^{2\gamma}$) are of comparable magnitude in the low-energy region of the potential, which yields a net interaction that goes to zero (or nearly to zero) in eclipsed conformations and produces a large splitting in the staggered conformations. In CH_3SH, the 1st-order interaction is dominant but changes sign near the equilibrium CXH bending angle, which leads to CIs on both staggered and eclipsed conformations. Recent results[23] show that CD_3OH also has a similar pattern of CIs which is between the adiabatic surfaces representing the asymmetric CD stretches and that their locations are close to those in CH_3OH. We have seen from a comparison of Figs. 2(a) and 2(b) that the CIs derive primarily from the variation of the single-bond force-constant in the large-amplitude space. This means that the CH bond force constants exhibit $\cos\gamma$ and $\cos 2\gamma$ variations with γ in the

1st- and 2nd-order Jahn-Teller interactions, respectively. A significant difference relative to the two methanol isotopologues is the larger size of the sulfur atom, which keeps the XH hydrogen about 0.5 Å further away from the methyl hydrogens in CH_3SH, and this could be connected with the relative weakness of the 2nd-order Jahn-Teller interaction in that molecule.

Xu, Hougen, and Lees[27] have reported an *ab initio* investigation of the CH stretch vibrations along the torsional minimum energy path of methanol. They discussed three limiting coupling cases:

Case 1: Only first-order Jahn-Teller coupling ($W^{1\gamma} \neq 0$; $W^{2\gamma} = 0$).
Case 2: Only second-order Jahn-Teller effect ($W^{1\gamma} = 0$; $W^{2\gamma} \neq 0$).
Case 3: First and second orders equal in magnitude ($W^{1\gamma} + W^{2\gamma} = 0$).

A fourth case, $W^{1\gamma} - W^{2\gamma} = 0$, was mentioned but not numbered. In all of these limiting coupling cases, the 4th-order ($W^{4\gamma}$) and higher Jahn-Teller couplings were assumed to be zero. They identified methanol as being close to Case 3, leading to a near-cancelation of the Jahn-Teller interactions at the torsional saddle point. Here, where we include a general dependence on ρ [any number of terms in Eq. (20)], the limiting cases are still useful points of reference. In CH_3OH, the Case 3 criterion becomes exact at the CIs located in the eclipsed geometry. In CH_3SH, the 2nd-order JT coupling is small, and Case 1 becomes a reasonable approximation.

The vibrationally adiabatic surfaces represented in Figs. 1(a) and 1(b) point to qualitative predictions about the nature of the infrared spectra of the two subject molecules in the CH-stretching region. For each molecule, the global equilibrium geometry is in the staggered conformation, with a substantially bent CXH angle, $\rho = 83°$ and 72° for CH_3SH and CH_3OH, respectively. Accordingly, the splitting of the adiabatic surfaces in this region will provide a measure of the expected splitting of the two asymmetric CH-stretch bands. In CH_3OH, the adiabatic surfaces are well separated in agreement with the traditional assignment, even in low-resolution spectra,[28] of the two asymmetric CH stretches as separate vibrational bands. High-resolution experiments[29,30] and full-dimensional theory[31–36] agree that the splitting between the two vibrations is in the range of 40–45 cm^{-1}. In CH_3SH, there is a CI near the global minimum energy geometry, and consequently the two adiabatic surfaces are nearly degenerate in that region. This implies that the fundamental frequencies of the two asymmetric CH stretches will be nearly degenerate. This expectation is supported by a recent high-resolution spectrum of CH_3SH,[37] which has the appearance of a single E-type perpendicular band characteristic of a degenerate CH stretch in a symmetric rotor. The high-resolution analysis indicates that the A' and A'' asymmetric stretches have a small splitting of 1–2 cm^{-1}. The qualitative appearance of the band as a degenerate perpendicular band results from the a-type Coriolis coupling which is much larger over the range of populated K-levels than the $J' = 0$ splitting of the A' and A'' components. Clearly, the arrangement of the conical intersections between the adiabatic surfaces, as modeled by the extended Jahn-Teller Hamiltonian, has a striking impact on the form of the infrared spectra.

In principle, the present extended Jahn-Teller model could serve as the starting point for a detailed simulation of the high-resolution spectra, but that would require a number of steps: (i) computation of the dynamical Jahn-Teller states including both slow and fast degrees of freedom, (ii) development of a torsion-vibration-rotation Hamiltonian based on the Jahn-Teller model, and (iii) inclusion of a zero-point average over the other 11 vibrations that are not treated explicitly in the present model.

As was elaborated in the previous work,[12,13] the present application of the Jahn-Teller Hamiltonian is predicated on an approximate separation of the high- and low-frequency vibrations and is therefore highly approximate. Most critically, the present examples retain only two high-frequency and two low-frequency degrees of freedom. The other 11 vibrational coordinates are represented only implicitly through the partial optimizations in the *ab initio* calculations, but then these coordinates are fixed allowing no further exploration of the potential or the dynamics in these degrees of freedom. Among the neglected phenomena are the stretch-bend resonances[38,39] and the interactions of the asymmetric CH stretched with the symmetric CH stretch (ν_3 in CH_3OH and ν_2 in CH_3SH).[12] The present applications are reduced-dimensional treatments that allow only certain aspects of the vibrational interactions to be quantified and visualized. The adiabatic concept is valuable, notwithstanding these limitations, because they provide a vocabulary and a frame of reference for describing important aspects of complex high-dimensional vibrational dynamics.

VI. SUMMARY

An expansion in the spherical harmonics has enabled an extension of the $E \otimes e$ Jahn-Teller Hamiltonian for treatment of nuclear motion that extends far from the 3-fold symmetric reference geometry. While this development is general, it is particularly applicable to the vibrational Jahn-Teller effect in molecules like CH_3SH and CH_3OH where the global minima on the electronic potential energy surfaces are far from the C_{3v} geometry. Both molecules have multiple conical intersections (CIs) between adiabatic surfaces representing the asymmetric CH stretch vibrations, but the arrangement of the CIs in configuration space is qualitatively different. That contrast is reflected in the experimental infrared spectra.

SUPPLEMENTARY MATERIAL

See supplementary material for the *ab initio* data and fit residuals for CH_3SH (Tables S1 and S2) and for their dependence on computational level (Table S3). Table S4 contains the parameters for a fit of the corresponding CH_3OH data to the present Hamiltonian.

ACKNOWLEDGMENTS

The authors are grateful to Marek Kreglewski and Tucker Carrington for their helpful suggestions. Support for this work was provided by the Division of Chemical Sciences, Offices of Basic Energy Sciences, Office of Energy Research,

U.S. Department of Energy under Grant No. DE-FG02-90ER14151.

[1] H. A. Jahn and E. Teller, Proc. R. Soc. A **161**, 220 (1937).
[2] *Conical Intersections: Theory, Computation and Experiment*, edited by W. Domcke, D. R. Yarkony, and H. Koeppel (World Scientific Publishing Co. Pte. Ltd., 2011), p. 754.
[3] I. B. Bersuker, *The Jahn-Teller Effect* (Cambridge University Press, 2006).
[4] J. W. Zwanziger and E. R. Grant, J. Chem. Phys. **87**, 2954 (1987).
[5] W. Eisfeld and A. Viel, J. Chem. Phys. **122**, 204317 (2005).
[6] A. Viel and W. Eisfeld, J. Chem. Phys. **120**, 4603 (2004).
[7] D. Opalka and W. Domcke, J. Chem. Phys. **132**, 154108 (2010).
[8] M. E. Kellman, Chem. Phys. Lett. **87**, 171 (1982).
[9] R. Marcus, J. Chem. Phys. **43**, 1598 (1965).
[10] M. Quack and J. Troe, Ber. Bunsengesellschaft Phys. Chem. **78**, 240 (1974).
[11] I. Smith, Acc. Chem. Res. **23**, 101 (1990).
[12] B. P. Thapaliya, M. B. Dawadi, C. Ziegler, and D. S. Perry, Chem. Phys. **460**, 31 (2015).
[13] M. B. Dawadi and D. S. Perry, J. Chem. Phys. **140**, 161101 (2014).
[14] J. von Neumann and E. Wigner, Phys. Z **30**, 467 (1929).
[15] M. A. Robb, M. Garavelli, M. Olivucci, and F. Bernardi, Rev. Comput. Chem. **15**, 87 (2007).
[16] B. G. Levine and T. J. Martinez, Annu. Rev. Phys. Chem. **58**, 613 (2007).
[17] D. R. Yarkony, Rev. Mod. Phys. **68**, 985 (1996).
[18] J. D. Coe and T. J. Martinez, J. Am. Chem. Soc. **127**, 4560 (2005).
[19] B. E. Applegate, T. A. Barckholtz, and T. A. Miller, Chem. Soc. Rev. **32**, 38 (2003).
[20] P. Hamm and G. Stock, Phys. Rev. Lett. **109**, 173201 (2012).
[21] P. Hamm and G. Stock, Mol. Phys. **111**, 2046 (2013).
[22] P. Hamm and G. Stock, J. Chem. Phys. **143**, 134308 (2015).
[23] E. M. Reid, L.-H. Xu, and R. M. Lees, "*Ab initio* study of fast small-amplitude vibrations as functions of slow large-amplitude motions in CD_3OH and comparison to CH_3OH," J. Mol. Spectrosc. (published online).
[24] L.-H. Xu, J. T. Hougen, R. M. Lees, and M. A. Mekhtiev, J. Mol. Spectrosc. **214**, 175 (2002).
[25] S. L. Altmann and C. J. Bradley, Philos. Trans. R. Soc., A **255**, 199 (1963).
[26] M. J. Frisch, G. W. Trucks, H. B. Schlegel, G. E. Scuseria, M. A. Robb, J. R. Cheeseman, G. Scalmani, V. Barone, B. Mennucci, G. A. Petersson, H. Nakatsuji, M. Caricato, X. Li, H. P. Hratchian, A. F. Izmaylov, J. Bloino, G. Zheng, J. L. Sonnenberg, M. Hada, M. Ehara, K. Toyota, R. Fukuda, J. Hasegawa, M. Ishida, T. Nakajima, Y. Honda, O. Kitao, H. Nakai, T. Vreven, J. A. Montgomery, Jr., J. E. Peralta, F. Ogliaro, M. J. Bearpark, J. Heyd, E. N. Brothers, K. N. Kudin, V. N. Staroverov, R. Kobayashi, J. Normand, K. Raghavachari, A. P. Rendell, J. C. Burant, S. S. Iyengar, J. Tomasi, M. Cossi, N. Rega, N. J. Millam, M. Klene, J. E. Knox, J. B. Cross, V. Bakken, C. Adamo, J. Jaramillo, R. Gomperts, R. E. Stratmann, O. Yazyev, A. J. Austin, R. Cammi, C. Pomelli, J. W. Ochterski, R. L. Martin, K. Morokuma, V. G. Zakrzewski, G. A. Voth, P. Salvador, J. J. Dannenberg, S. Dapprich, A. D. Daniels, Ö. Farkas, J. B. Foresman, J. V. Ortiz, J. Cioslowski, and D. J. Fox, GAUSSIAN 09, Revision B.0.1, Gaussian, Inc., Wallingford, CT, USA, 2009.
[27] L.-H. Xu, J. T. Hougen, and R. M. Lees, J. Mol. Spectrosc. **293-294**, 38 (2013).
[28] A. Serrallach, R. Meyer, and H. H. Gunthard, J. Mol. Spectrosc. **52**, 94 (1974).
[29] L.-H. Xu, X. Wang, T. J. Cronin, D. S. Perry, G. T. Fraser, and A. S. Pine, J. Mol. Spectrosc. **185**, 158 (1997).
[30] X. Wang and D. S. Perry, J. Chem. Phys. **109**, 10795 (1998).
[31] E. L. Sibert III and J. Castillo-Chara, J. Chem. Phys. **122**, 194306 (2005).
[32] J. M. Bowman, T. Carrington, and H.-D. Meyer, Mol. Phys. **106**, 2145 (2008).
[33] J. M. Bowman, X. Huang, N. C. Handy, and S. Carter, J. Phys. Chem. A **111**, 7317 (2007).
[34] L.-H. Xu, R. M. Lees, J. T. Hougen, J. M. Bowman, X. Huang, and S. Carter, J. Mol. Spectrosc. **299**, 11 (2014).
[35] S. Blasco and D. Lauvergnat, Chem. Phys. Lett. **373**, 344 (2003).
[36] D. Lauvergnat and A. Nauts, Spectrochim. Acta, Part A **119**, 18 (2014).
[37] B. G. Guislain, E. M. Reid, R. M. Lees, L.-H. Xu, S. Twagirayezu, D. S. Perry, B. P. Thapaliya, M. B. Dawadi, and B. E. Billinghurst, J. Mol. Spectrosc. **335**, 37 (2017).
[38] S. Twagirayezu, T. N. Clasp, D. S. Perry, J. L. Neill, M. T. Muckle, and B. H. Pate, J. Phys. Chem. A **114**, 6818 (2010).
[39] S. Twagirayezu, X. Wang, D. S. Perry, J. L. Neill, M. T. Muckle, B. H. Pate, and L.-H. Xu, J. Phys. Chem. A **115**, 9748 (2011).